

## Detection of shallow inclusions in closed-packed granular beds using mechanical impulses

Saravanan Swaminathan and Donald P. Visco, Jr.

Department of Chemical Engineering, Tennessee Technological University, Cookeville, Tennessee 38505

Surajit Sen<sup>a)</sup>

Physics Department, State University of New York, Buffalo, New York 14260

(Received 10 September 2006; accepted 12 March 2007; published online 12 April 2007)

Mechanical energy has been used in the detection of shallow buried objects in granular beds for more than half a century. Here we attempt to answer a fundamental question—at what depths would an object be detectable in an idealized, close-packed, granular bed made of monosized elastic spheres? Systematic particle dynamics based studies reveal the effects of varying the area across which the impulse is generated, object size, and restitution on locating the buried object. © 2007 American Institute of Physics. [DOI: 10.1063/1.2722194]

The problem of acoustically detecting *shallow*, buried objects in granular beds has a rich history.<sup>1–8</sup> There are even accounts from the life sciences about how doodlebugs or antlions survive in the soil using sound waves.<sup>9</sup> Much of the work has been done by those involved in acoustic land mine detection and is largely experimental and records of conference presentations<sup>1,10</sup> and often without reference to studies from the academic communities. As a result, well known issues such as the inadequacy of the wave equation to describe mechanical energy propagation<sup>11</sup> through shallow soil have been often ignored in much of the existing literature.<sup>1,2,8,10</sup>

There are a few experimental studies of impulse propagation at shallow depths of granular beds.<sup>7,8,12</sup> These demonstrate that energy propagation is sensitive to packing and is not like wave propagation by revealing that the signal speed depends upon amplitude and that signal dispersion is limited.<sup>12</sup> Here we address a fundamental question—at what depths would an object be detectable in an idealized, close-packed, granular bed made of monosized elastic spheres? To answer this question, one must consider the velocity perturbation imparted to the surface grains, the perturbation area, obstacle size, obstacle depth, the nature of granular contacts, and the amount of restitutive loss.<sup>13</sup>

We consider the propagation of a velocity perturbation imparted onto a fixed area  $A$  ( $\equiv L \times L$ ), measured in grain diameters, as shown in Fig. 1(a). Detection of shallow objects, which are likely to produce significant backscattering, is a challenge. To study this, we create a system comprised of  $40 \times 40 \times 60$  monodisperse quartz spheres of radius  $R$  grains in a hexagonal-close-packed (hcp) lattice.<sup>13</sup> The spheres interact upon compression via the nonlinear Hertz potential<sup>14</sup>  $V(\delta_{ij}) = a\delta_{ij}^{3/2}$ , where  $a = (2/5D)(R/2)^{1/2}$ ,  $R = 0.5 \times 10^{-4}$  m,  $D \equiv 3(1 - \sigma^2)/2Y$ ,  $Y = \text{Young's modulus}$  ( $7.8 \times 10^{10}$  N m<sup>-2</sup>),  $\sigma = 0.144$  is Poisson's ratio for quartz, and the grain overlap parameter  $\delta_{ij} \equiv 2R - (|\mathbf{r}_i - \mathbf{r}_j|) \geq 0$ , where  $(i, j)$  are neighbors in contact in the hcp lattice. Such a potential is steeper than harmonic at large enough compressions but is softer than harmonic at small compressions. This potential, along with

the requirement of momentum conservation, leads to effectively ballistic-like energy transport.<sup>12,13</sup>

We set the velocity of all the grains to be zero at  $t=0$  except for those centered on an area  $A$  at the bed surface. All subsequent grain positions, velocities, and accelerations are computed by numerically integrating the equation of motion for each grain via the velocity-Verlet algorithm<sup>15</sup> using a  $0.1 \mu\text{s}$  time step of integration. A larger time step introduces errors and a smaller time step does not yield significant benefits. The perturbation propagates as a compression pulse into the system. The effect of restitution ( $e$ ) is included via the intergrain force during loading and unloading,<sup>16</sup>  $F_{\text{unload}}/F_{\text{load}} \equiv 1 - e$ , where  $0 < e < 1$  defines the restitution

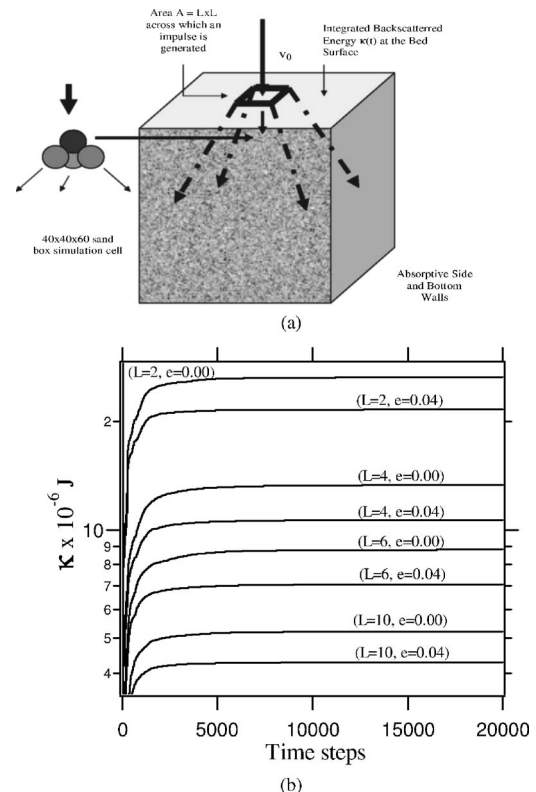


FIG. 1. (a) Schematic diagram of the system. (b) Effect of restitution ( $e$ ) on  $\kappa$  for different impulse areas ( $L$ ). Note that no obstacle is present in the bed.

<sup>a)</sup> Author to whom correspondence should be addressed; electronic mail: sen@nsm.buffalo.edu

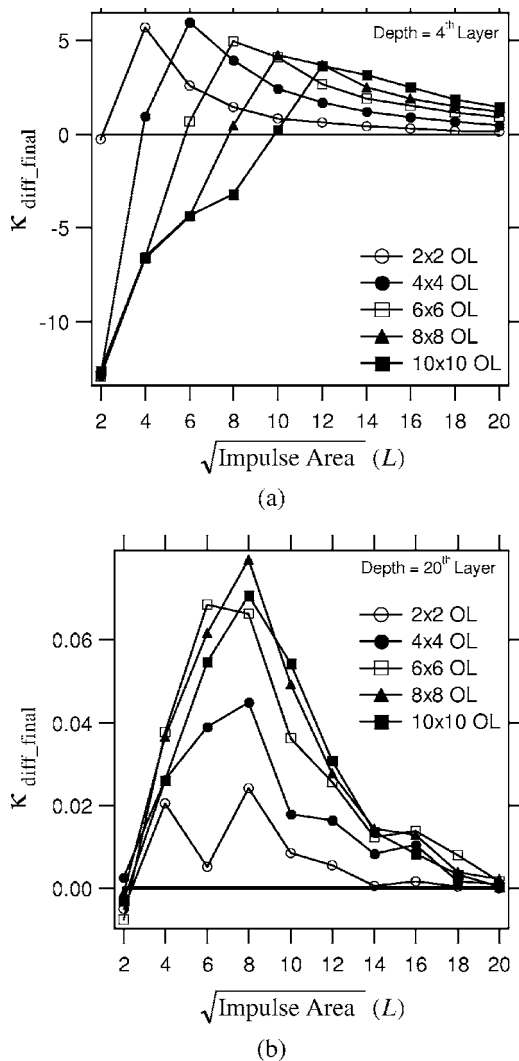


FIG. 2. (a)  $\kappa_{diff\_final}$  vs impulse area for five different obstacle areas (OL=2, 4, 6, 8, and 10) at layer 4. (b)  $\kappa_{diff\_final}$  vs impulse area for five different obstacle areas (OL=2, 4, 6, 8, and 10) at layer 20.

parameter with  $F_{load}(F_{unload})$  referring to the (de)compression force between two grains in contact. Hence,  $e=0(1)$  denotes completely (in)elastic behavior. To avoid wall reflection effects, the four sidewalls and the bottom wall are made completely *energy absorptive*. To study a range of impulse areas, we use  $L=2, 4, 6, 8, 10, 12, 14, 16, 18,$  and  $20$  (in grain diameters) while using a variety of obstacle areas OA ( $\equiv OL \times OL$ ) where  $OL=2, 4, 6, 8,$  and  $10$ . Additionally, to explore the effects of restitution, we let  $e=0$  and  $0.04$  (4% restitution).

The impulse is initiated across an area of the surface. The energy spreads in a cone-shaped form as sketched in Fig. 1(a). Impulse velocities of 5 and 50 m/s were used to study the cumulative backscattering at the second layer. It was found that for the case of 5 m/s, the backscattering was too weak to be easily detected and, thus, we decided to use an impulse velocity of 50 m/s. In this work, we examine the time integrated or cumulative kinetic energy at the surface. We define the cumulative average kinetic energy per surface grain  $\kappa(t) \equiv \sum_0^t (1/N_s) \sum_N p_i^2(\tau) / 2m$ , where  $N_s$  is the number of surface grains,  $\tau$  is a dummy variable for time, and  $\kappa(t)$  is averaged over all time from  $\tau=0$  to  $\tau=t$ . Figure 1(b) illustrates the dynamic behavior of  $\kappa(t)$  for a few represen-

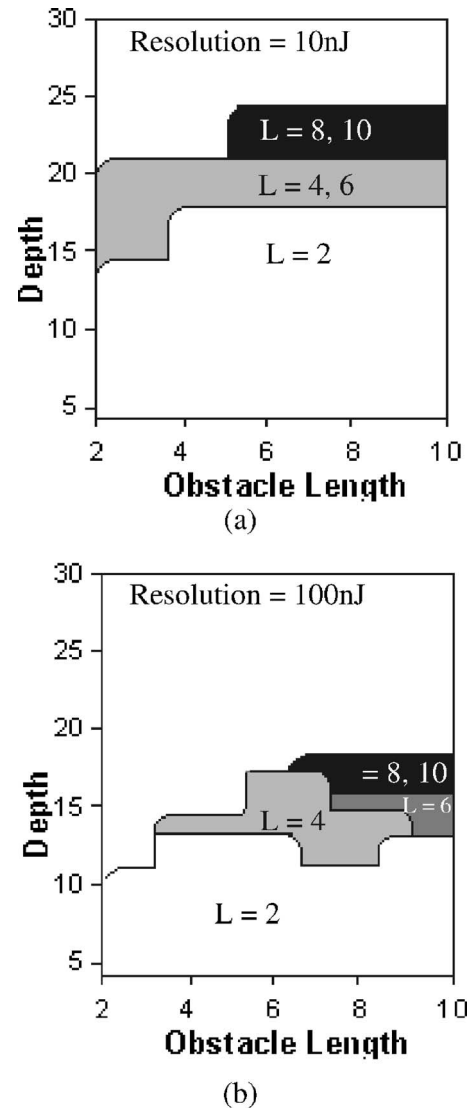


FIG. 3. (a) Global phase diagram without restitution for a resolution of 10 nJ. (b) Global phase diagram without restitution for a resolution of 100 nJ.

tative impulse areas. Note that  $\kappa$  reaches a quick *minimum* as the energy enters into the bed and then grows in time to reach an asymptotic value  $\kappa_{final}$ . Figure 1(b) confirms  $\kappa_{final} L = \text{constant}$ .<sup>13</sup> The larger the  $L$ , the less is the energy backscattered to the surface. Further, introducing restitution reduces the magnitude of  $\kappa_{final}$ .

Having characterized the dynamics of the empty bed, we introduce the object to be detected. Here we examine all combinations of object size ( $OL=2, 4, 6, 8,$  and  $10$ ), object location (layer depth= $4, 6, 8, 10, 12, 14, 16, 18, 20, 25,$  and  $30$ ), and impulse area ( $L=2, 4, 6, 8, 10, 12, 14, 16, 18,$  and  $20$ ). Since we are interested in the effect of the presence of the obstacle on backscattered energies, we calculate a  $\kappa_{diff\_final} (\equiv \kappa_{final \text{ bed (with obstacle)}} - \kappa_{final \text{ (without obstacle)}}$ ), which is the difference in  $\kappa_{final}$  between the pure bed and that with the obstacle. The  $\kappa_{diff\_final}$  values for all cases can be found elsewhere.<sup>17</sup>

Ultimately, we determine if the object is detectable by analyzing the values of  $\kappa_{diff\_final}$ . If  $\kappa_{diff\_final} < 0$ , it is an indication that the impulse area is smaller than the obstacle area resulting in a reduction of the number of particles participating in the backscattering. Here, many layers of grains

directly beneath the object are effectively shielded from the impulse. If  $\kappa_{\text{diff\_final}} > 0$ , it indicates that the backscattering from the buried object exceeds the ambient backscattering present from the empty bed. Figure 2 illustrates the profile of  $\kappa_{\text{diff\_final}}$  when placing the obstacle at two representative layers. It can be seen in Fig. 2(a) that there is a peak for every obstacle area near the value of the impulse area. This indicates that at shallow depths (layer=4), we get maximum backscattering for the cases when  $L \geq OL$ . The other key feature that can be seen in Fig. 2(a) is that  $\kappa_{\text{diff\_final}}$  values cross over from the negative to the positive region when the  $L \approx OL$ . Figure 2(b) depicts the trend of  $\kappa_{\text{diff\_final}}$  values when the obstacles are placed in the 20th layer. It can be seen that the peak in this case occurs when  $L > OL$ . This is due to the fact that as the obstacle depth is increased, there is an attenuation in the magnitude of the  $\kappa_{\text{diff\_final}}$  which, in turn, leads in requiring larger impulse areas to detect the presence of smaller obstacles.

To form an overall picture of the ability to detect the smallest object using different impulse areas, larger scale dynamical studies are warranted. However, global “phase diagrams” for small systems can be constructed, as in Fig. 3, by performing many simulations using various impulse areas and obstacle lengths. As there are sensors that can detect energies of 0.2 pJ,<sup>18</sup> these diagrams have been constructed for two reasonable energy “resolutions,” 10 and 100 nJ (where resolution defines the smallest detectable energy), for the values of  $\kappa_{\text{diff\_final}}$  at long enough times (i.e.,  $2 \times 10^4$  time steps). The results in Fig. 3 are for  $e=0$ . The different regions shown with different shades indicate the detectability of the different obstacle areas using representative impulse areas. Note that negative values of  $\kappa_{\text{diff\_final}}$  can be detected (if greater than the resolution) since this value is not a negative absolute energy, but relative to that of the empty bed. In each of these cases, the values of  $\kappa_{\text{diff\_final}}$  depend on whether or not restitutional losses are present. We find that as the resolution increases, there is significant change in the phase diagram for a selected impulse area. Note that a tighter resolution changes the detectable ranges, but not the nature of the curves. Also, the incorporation of restitution at 4% has negligible change on these diagrams.

We have studied the detectability of small buried objects at shallow depths using backscattering of different mechanical impulses across small areas. The results are shown by constructing global phase diagrams. Our study suggests that there exists a relationship between the size of the impulse area and the size of the obstacle area, a result that may be vital for detectability of small buried objects at shallow depths.

The authors thank ARO and NSF for partial support.

<sup>1</sup>There are several reports on buried object detection that are not refereed contributions but are available, e. g., J. F. Mifsud, University of Texas Report No. DRL-A-95, 1955 (unpublished); S. Rickser, University of Texas Report No. DRL-A-98, 1955 (unpublished); D. A. Sachs, B. G. Watters, P. K. Krumhansel, P. W. Smith, J. Doherty, J. Webb, and A. Davidson, BBN Technical Report No. 7677, submitted to the U.S. Army Belvoir Research and Development Center, 1992 (unpublished), Vols. 1–3.  
<sup>2</sup>J. C. Cook and J. J. Wormser, IEEE Trans. Geosci. Electron. **GE11**, 135 (1973).

<sup>3</sup>A. Shukla and C. Damania, Exp. Mech. **27**, 268 (1987).

<sup>4</sup>C. Y. Zhu, A. Shukla, and M. H. Sadd, J. Appl. Mech. **58**, 341 (1991).

<sup>5</sup>A. J. Rogers and C. G. Don, Acoust. Aust. **22**, 5 (1994).

<sup>6</sup>R. S. Sinkovits and S. Sen, Phys. Rev. Lett. **74**, 2686 (1995).

<sup>7</sup>A. Britan, G. Ben-Dor, T. Elperin, O. Igra, and J. P. Jiang, Exp. Fluids **22**, 432 (1997).

<sup>8</sup>G. S. Baker, C. Schmeissner, D. W. Steeples, and R. G. Plumb, Geophys. Res. Lett. **26**, 279 (1999).

<sup>9</sup>J. T. Botz, C. Loudon, J. B. Barger, J. S. Olafsen, and D. W. Steeples, Integr. Comp. Biol. **42**, 6 (2002).

<sup>10</sup>There are several SPIE Conference Proceedings with reports on work on acoustic land mine detection, see, for example, A. Dubey, J. Harvey, J. T. Broach, and V. George, Proc. SPIE **4394** (2001).

<sup>11</sup>S. Sen, T. R. Krishna Mohan, D. P. Visco, Jr., S. Swaminathan, A. Sokolow, E. Avalos, and M. Nakagawa, Int. J. Mod. Phys. B **19**, 2951 (2005), and references therein.

<sup>12</sup>S. R. Hostler and C. E. Brennen, Phys. Rev. E **72**, 031303 (2005); **72**, 031304 (2005).

<sup>13</sup>D. P. Visco, Jr., S. Swaminathan, T. R. Krishna Mohan, A. Sokolow, and S. Sen, Phys. Rev. E **70**, 051306 (2004).

<sup>14</sup>H. Hertz, J. Reine Angew. Math. **92**, 156 (1881).

<sup>15</sup>M. P. Allen and D. J. Tildesley, *Computer Simulation of Liquids* (Clarendon, Oxford, 1987), pp. 71–84

<sup>16</sup>O. R. Walton and R. L. Braun, J. Rheol. **30**, 949 (1986).

<sup>17</sup>[http://electron.physics.buffalo.edu/~sen/documents/apl\\_don\\_Supplemental\\_Material.pdf](http://electron.physics.buffalo.edu/~sen/documents/apl_don_Supplemental_Material.pdf)

<sup>18</sup><http://www.coherentinc.com/Lasers/index.cfm?fuseaction=show.page/id=961>